Workshop on Astrophysical Opacities
ASP Conference Series, Vol. 515
C. Mendoza, S. Turck-Chièze, and J. Colgan, eds.

Recalculation of Astrophysical Opacities: Overview, Methodology, and Atomic Calculations

Anil K. Pradhan and Sultana N. Nahar

Dept. of Astronomy, The Ohio State University, Columbus, OH 43210, USA
pradhan.1@osu.edu

Abstract. We present a review of a renewed effort to recalculate astrophysical opacities using the *R*-Matrix method, describing the computational methods and new extensions. Resulting enhancements relative to the Opacity Project found in test calculations under stellar interior conditions could potentially lead to the solution of the solar abundance problem, as well as the discrepancies between recent experimental measurements at the Sandia Z-pinch inertial confinement fusion device and theoretical opacity models. Outstanding issues also discussed are: (i) accuracy, convergence, and completeness of atomic calculations; (ii) improvements in the equation of state of high-temperature-density plasmas; (iii) redistribution of resonant oscillator strength in the bound–free continuum, and (iv) plasma broadening of autoionizing resonances.

1. Introduction

The Opacity Project was launched in 1983 with the goal of calculating astrophysical opacities using state-of-the-art atomic physics based on the coupled channel (CC) approximation employing the powerful *R*-Matrix (RM) method (Seaton et al. 1994; The Opacity Project Team 1995, 1997). Over the next decade, a suite of extended RM opacity codes were developed to compute large-scale bound–bound (bb) transition strengths and bound–free (bf) photoionization cross sections with unprecedented accuracy. One of the primary features of the OP was the precise delineation of intrinsic autoionizing resonance profiles whose shapes, extent, and magnitudes are determined by myriad channel couplings in the electron+ion system.

However, CC-RM calculations are of immense complexity and require substantial computational effort and resources. For the often dominant inner-shell transitions, they could not be completed due to computational constraints on the then available high-performance computing platforms. Simpler approximations, akin to distorted-wave (DW) type methods used in other opacity models that neglect channel couplings, were therefore employed to compute most of the OP data.

In recent years a renewed effort has been under way as originally envisaged using the CC-RM methodology (Nahar & Pradhan 2016a, hereafter NP16a) stimulated by two independent developments. The first was a 3D non-LTE analysis of solar elemental abundances that were up to 50% lower for common volatile elements such as C, N, O, and Ne (Asplund et al. 2009). It was suggested that an enhancement of up to 30% in the opacities could resolve this discrepancy, particularly in helioseismological models (Turck-Chièze 1998; Turck-Chièze et al. 2004; Bahcall et al. 2005; Basu & Antia 2008; Christensen-Dalsgaard et al. 2009, J. Bahcall, private communication). The second

was an experimental measurement of the iron opacity at the Sandia Z-pinch inertial confinement fusion device under stellar interior conditions prevalent at the base of the solar convection zone (BCZ), which was 30–400% higher in monochromatic opacity compared to OP (Bailey et al. 2015). The Z-pinch results for the Rosseland mean opacity (RMO) were also substantially higher and nearly half the enhancement needed to resolve the solar abundance problem.

The pilot CC-RM calculations in NP16a for an important iron ion, Fe XVII, resulted in a 35% enhancement relative to the OP RMO at the Z conditions. While the enhancement is consistent with subsequently reported results from other opacity models (Blancard et al. 2016; Nahar & Pradhan 2016b), there are also important differences in (i) the atomic physics, (ii) equation of state, and (iii) plasma broadening of autoionizing resonances. The Fe XVII calculations were carried through to convergence by including $n = 3$ and $n = 4$ levels of the Fe XVIII target ion. They showed large enhancements in the photoionization cross sections as successive thresholds were included due to coupled resonance structures and the background.

The extensive role of the *photoexcitation-of-core* (PEC) resonances (also known as Seaton resonances, Yu & Seaton 1987) associated with strong dipole transitions in the Fe XVIII core ion is especially prominent (NP16a). Several other sets of the pilot calculations have been carried out: relativistic Breit–Pauli *R*-Matrix (BPRM) calculations including 60 fine-structure levels up to the $n = 3$ thresholds; non-relativistic calculations including 99 LS terms up to the $n = 4$ thresholds; as well as BPRM calculations with 218 fine-structure levels (in progress). One of the aims is to benchmark existing DW cross sections and monochromatic opacities in the non-resonant background and high-energy region above all coupled excitation thresholds.

Small wave-function expansions for the e+ion system in the *R*-Matrix calculations were among the compromises necessary in the initial OP work, usually limited to the ground configuration of the core ion. One of the main points of the NP16a work was that, *in general for any atomic system, a converged expansion in terms of the target configurations and levels is needed to include the full enhancement of the photoionization cross sections for each level in the bf continuum*.

We are currently investigating the occupation probabilities from the Mihalas–Hummer–Dappen equation of state (MHD-EOS) employed in the OP work, which are orders of magnitude lower for excited levels than other models. Also a new theoretical method and computational algorithm for electron impact broadening of autoionizing resonances in plasmas as a function of temperature and density has been developed; and finally, we are addressing issues related to completeness and accuracy. The following sections describe some of the salient features of the work outlined above.

2. Close-Coupling and Distorted-Wave Approximations

The close-coupling approximation is implemented using the CC-RM method. It involves the expansion of the total wave function for the e+ion system in terms of the eigenfunctions of the "target" ("core") ion states and a free-electron function

$$\Psi(E) = \mathcal{A} \sum_i \chi_i \theta_i + \sum_j c_j \Phi_j \, , \tag{1}$$

where χ_i is the target-ion wave function in a specific $S_i L_i$ state, and θ_i is the wave function for the free electron in a channel labeled $S_i L_i k_i^2 \ell_i (S L \pi)$, k_i^2 being its incident kinetic

energy. In contrast to the CC-RM method, the DW approximation used in other opacity models neglects the summation over the hundreds to thousands of channels of Eq. (1). In essence that implies the neglect in the DW method of the quantum superposition and interference that gives rise to autoionizing resonances in an *ab initio* manner.

To obtain bb, bf, and scattering matrix elements, we obtain e+ion wave functions $\Psi_B(S\,L\pi; E)$ and $\Psi_F(S\,L\pi; E')$. For bound states B and B' the line strength in a.u. is given by

$$\Gamma(B; B') = |\langle\Psi_B(E_B)||\mathbf{D}||\Psi_{B'}(E_{B'})\rangle|^2 \tag{2}$$

where **D** is the dipole operator. If the final state is a continuum state represented by $\Psi_F(E')$ and the initial state by $\Psi_B(E)$, the photoionization cross section is then given by

$$\sigma_\omega(B; E') = \frac{4}{3}\frac{\alpha\omega}{g_i}|\langle\Psi_B(E_B)||\mathbf{D}||\Psi_F(E')\rangle|^2 \tag{3}$$

where ω is the photon frequency and E' is the energy of the outgoing electron. The relativistic BPRM method incorporates the Breit–Pauli Hamiltomian for the $(N + 1)$-electron system, and we employ a pair-coupling representation $S_iL_l(J_i)l_i(K_i)s_i(J\pi)$. As the individual states S_iL_i split into the fine-structure levels J_i, the number of channels becomes several times larger than the corresponding LS coupling case. Hitherto, the version of BPRM codes included only the one-body terms of the Breit interaction, namely, the spin–orbit coupling, mass correction, and Darwin terms (Eissner 1991). Chen and Eissner (to be published) have developed an improved Breit–Pauli version including the two-body terms in the Breit interaction (see Fig. 1), which should be more accurate for fine-structure and resonance effects in the Fe-group elements.

3. R-Matrix Opacity Codes

The *R*-Matrix opacity codes (Berrington et al. 1987; Seaton 1987) are significantly different from the original *R*-Matrix codes of Burke (2011), and have been considerably extended by our group at Ohio State University for complete RM opacity calculations (Figs. 1–2). Fig. 1 is a flowchart of the RM codes set up and used at the Ohio Supercomputer Center (OSC) since 1990. An accurate configuration-interaction representation of the core-ion states is obtained by two atomic structure codes: SUPERSTRUCTURE (Eissner et al. 1974) and CIV3 (Hibbert 1975). The first two *R*-Matrix codes, STG1 and STG2, are then employed to generate the multipole integrals and algebraic coefficients and to set up the $(N + 1)$-electron Hamiltonian corresponding to the coupled integro-differential equations. The Hamiltonian is diagonalized in STGH (in the BP calculations diagonalization is preceded by $LS\,J$ recoupling in RECUPD). The *R*-Matrix basis set of functions and dipole matrix elements so produced are then input into STGB for bound-state wave functions, STGF for continuum wave functions, STGBB for radiative transition probabilities, and STGBF for photoionization cross sections. In addition, STGF(J) is used to obtain collision strengths for electron impact excitation in LS or intermediate coupling.

The flowchart of the new package of codes for opacity calculations is shown schematically in Fig. 2; each of the boxes represents a series of subsidiary codes. The new version of the *R*-Matrix opacity codes is the extension of the following codes under development: INTFACE interfaces atomic data for bf photoionization and bb transition probabilities including relativistic fine structure; AUTOBRO, an algorithm for electron

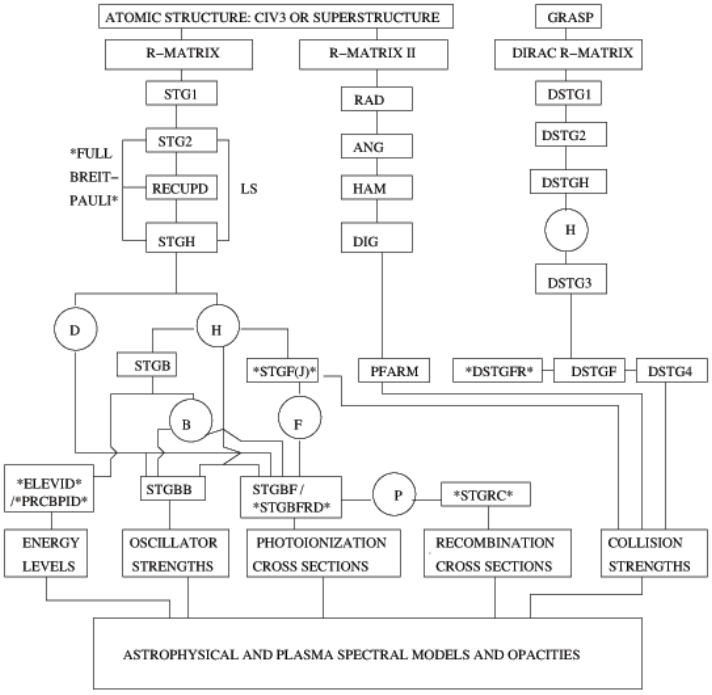

Figure 1. *R*-Matrix codes for the calculation of opacities. The left branch of the Breit–Pauli codes is employed in the results presented in this work.

impact broadening of autoionizing resonances with a temperature–density dependent kernel; and HIPOP, a high-precision version of the opacity code with high-resolution (10^5 frequencies) and monochromatic opacities and Rosseland and Planck mean opacities for arbitrary mixtures. The opacity database OPSERVER is described by Mendoza et al. (2007) with a recent update by Delahaye et al. (2016).

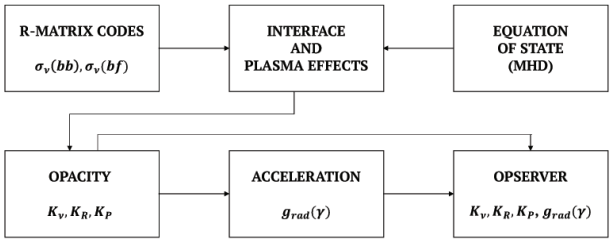

Figure 2. Opacity codes including interfaces with CC-RM data and the equation-of-state calculations.

4. Inner- and Outer-Shell Excitations

The CC-RM approach entails an increasing succession of open channels as each threshold of the core ion is approached from below (Eq. 1). As the number of free channels (open + closed) multiplies, the sizes of the e+ion algebra and *R*-Matrix diagonaliza-

tion matrices and arrays may become very large. Moreover, there are issues related to spectroscopic identification of highly excited and mixed-configuration bound e+ion levels from STGB calculations and subsequent bb STGBB and bf STGBF calculations (Fig. 1). While these have been solved, they require commensurate computational resources and expertise.

Inner-shell excitations using the DW method have been described in earlier works (e.g., Badnell & Seaton 2003). Despite the fact that most of current OP data was computed using variants of DW data, the initial OP calculations were done using the RM method, albeit with relatively small eigenfunction expansions and only a few outer-shell excitations. Most of the OP codes were originally developed to employ the RM methodology, but computational constraints precluded OP work from incorporating resonant inner-shell atomic processes that manifest themselves strongly in the bf cross sections. However inner-shell excitations are dominant contributors to the opacity because most electrons in complex ions are in closed shells, whose excitation energies lie above the (first) ionization threshold. Much of the opacity therefore lies in the strongest such transitions that are associated with dipole transitions in the ion core, i.e., the PEC resonances discussed extensively by Yu & Seaton (1987), Nahar et al. (2011), Pradhan & Nahar (2011), and NP16a. *The PEC resonances are the largest single contributing feature to the bf opacity.* Therefore their simple treatment as bb transitions in DW opacity models needs verification.

5. New R-Matrix Opacity Calculations: Test Case of Fe XVII

The monochromatic opacity comprises of bb, bf, free–free (ff), and photon scattering (sc) contributions:

$$\kappa_{ijk}(\nu) = \sum_k A_k \sum_j F_j \sum_{i,i'} [\kappa_{bb(}(i,i';\nu) + \kappa_{bf}(i,\epsilon i';\nu) + \kappa_{ff}(\epsilon i,\epsilon' i';\nu) + \kappa_{sc}(\nu)] \ , \quad (4)$$

where A_k is the abundance of element k, F_j the j ionization fraction, i and i' are the initial bound and final bound/continuum states of the atomic species, and ϵ represents the electron energy in the continuum. The κ_R RMO is defined in terms of $\kappa_{ijk}(\nu)$ as

$$\frac{1}{\kappa_R} = \frac{\int_0^\infty g(u)\kappa_\nu^{-1} du}{\int_0^\infty g(u) du} \quad \text{with} \quad g(u) = u^4 e^{-u}(1-e^{-u})^{-2}, \quad (5)$$

where $g(u)$ is the derivative of the Planck weighting function (corrected for stimulated emission), $\kappa_{bb}(i,i') = (\pi e^2/m_e c) N_i f_{ii'} \phi_\nu$, and $\kappa_{bf} = N_i \sigma_\nu$. The κ_ν is then primarily a function of the bb oscillator strengths f, bf photoionization cross sections σ_ν, level populations N_i, and the line-profile factor ϕ_ν. The CC-RM framework for large-scale computations comprises mainly the first two components of the opacity in Eq. (4): (i) the bb transition probabilities and (ii) the bf photoionization cross sections.

We focus on test calculations for an important contributor to the opacity at the Z-pinch plasma conditions: $T = 2.11\times10^6$ K and $N_e = 3.1\times10^{22}$ cm^{-3}. The experimental energy range and the range of the Planck function derivative dB/dT is shown in the right panel of Fig. 3. The Fe XVII calculations involved the coupled channel wavefunction expansion in Eq. (1) including 30 LS terms with 60 fine-structure levels up to the $n \leq 3$ complex of the core ion Fe XVIII (Nahar et al. 2011), and 99 LS terms

or 218 levels up to $n \leq 4$ (NP16a); the latter calculation was an order of magnitude larger computationally. The associated $n = 2 \rightarrow 3$ core transitions in Fe XVIII in the former case and the $n = 2 \rightarrow 3, 4$ in the latter give rise to numerous PEC resonances in the bf photoionization cross sections of Fe XVII. Fig. 3 (left) from NP16a compares the enhancement in the new cross sections compared to the two-state coupled channel results from OP that reproduce only the background. There is no "misrepresentation" of OP as has been asserted (Iglesias & Hansen 2017, hereafter IH17) since that is the only other CC calculation available; the rest of the OP work is DW.

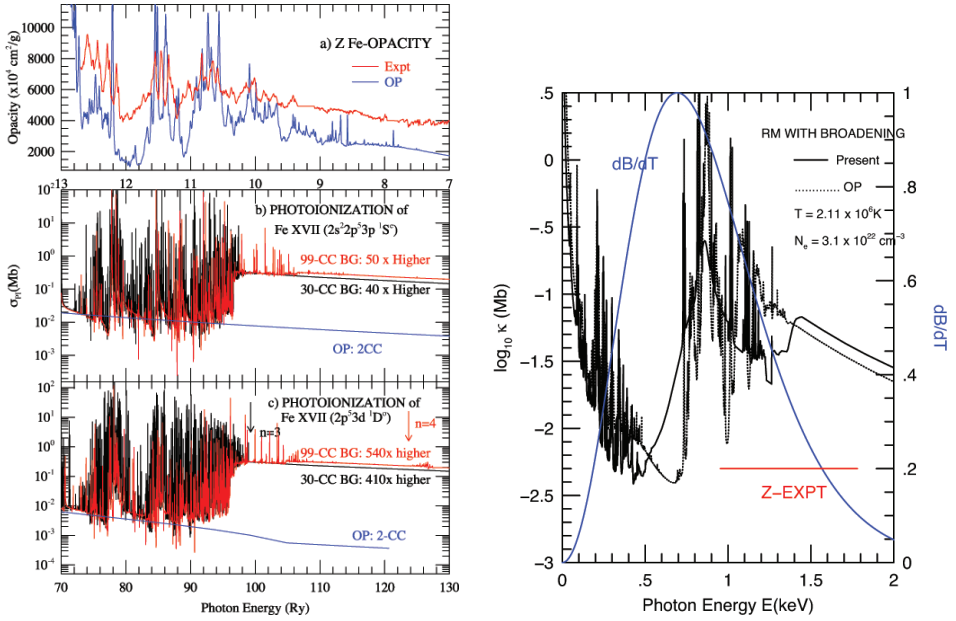

Figure 3. *Left*: Autoionizing resonance structures in *R*-Matrix photoionization cross sections of two Fe XVII excited levels (*bottom* and *middle panels*); "higher-than-predicted" Sandia Z-pinch measurements of total Fe opacity (*top panel*, Bailey et al. (2015). Calculations are needed for Fe XVI – Fe XXI to compare with experiments at Z plasma conditions. [Reproduced from Fig. 3 of Nahar & Pradhan (2016a), Copyright (2016), by permission of the American Physical Society.] *Right:* Monochromatic *R*-Matrix opacity of Fe XVII at $T = 2.11{\times}10^6$ K and $N_e = 3.1{\times}10^{22}$ cm^{-3} corresponding to total iron opacity measurements at the Sandia Z-pinch fusion device in the energy range shown by the red bar (*left panel*); the *R*-Matrix Fe XVII RMO is ~60% higher than OP (Table 1).

6. Convergence and Completeness

The two criteria for *accuracy and completeness* of the RM opacity calculations are: (i) *convergence* of the wave-function expansion (Eq. 3) with respect to bf cross sections and bb transition probabilities; and (ii) *completeness* of monochromatic opacities and RMOs with respect to a very large number of possible multiply excited configurations that contribute to the background non-resonant cross sections in high-temperature plasmas. The NP16a work demonstrated convergence with respect to the Fe XVIII target ion

included in the CC-RM calculations (Fig. 3, left), but the highly excited configurations that affect the high-energy behavior were not included.

Although the number of these excited configurations is large, their contribution to the opacity is still small relative to the main CC-RM cross sections. It is also specific to the energy range where the quasi-degenerate configurations lie. Additionally, they represent the background contribution without resonances, thus amenable to simpler approximations such as the DW without loss of accuracy. We refer to these configurations as the "top-up" contribution to the CC-RM calculations.

While enumerating excited configurations is straightforward in an atomic structure-DW calculation (IH17; Zhao et al. 2018), it is more complex and indirect in CC-RM calculations owing to resonant phenomena. (IH17 incorrectly stated that some of configurations were omitted in NP16a; in fact the $nl = 4d, 4f$ are included.) For example, the 60CC, $n \leq 3$ BPRM calculations yield 454 bound levels for Fe XVII, but we have further included $> 50\,000$ top-up levels to compute the opacity spectrum in Fig. 3 (right). However, the photoionization cross sections of the 454 strictly bound levels (negative eigenenergies) take into account embedded autoionizing resonances that are treated as distinct levels in DW calculations; therefore, in total there are commensurate number of levels to ensure completeness. Zhao et al. (2018) discuss the complementary top-up to the CC-RM calculations and find a ∼20% increment. Satisfying both these criteria results in a further enhancement in the Fe XVII RMO over that obtained in NP16a of ∼60% over OP. Table 1 shows the latest CC-RM results compared to other models. We expect additional enhancement upon completion of the $n = 4$ fine-structure calculations, which is likely the cause of the deficit in monochromatic opacity just below 1.5 keV in Fig. 3 (left). Updated results will be presented in Pradhan et al. (2018).

Table 1. Fe XVII RMO enhancement factors relative to OP for recent *R*-Matrix results (60% higher, Pradhan et al. 2018) and other opacity models employing variants of the DW method (Blancard et al. 2016). Further enhancement in the *R*-Matrix opacities is expected after proposed improvements in more extended atomic calculations and the MHD-EOS.

Method	Enhancement Factor
R-Matrix	1.64
OPAS	1.55
SCO-RCG	1.37
ATOMIC	1.32
SCRAM	1.27
TOPAZ	1.21

7. Differential Oscillator Strength Distribution and Sum Rule

The oscillator strength sum rule is invoked to ensure completeness. The summation over all bb and bf transitions must satisfy the condition built into the definition of the oscillator strength as a fractional excitation probability: $\sum_j f_{ij} = N$, where N is the number of active electrons. However, while the f-sum rule ensures completeness, it does not relate to the accuracy of atomic calculations per se. Rather, it is the precise energy distribution of differential oscillator strength that is the accuracy determinant. To wit: a hydrogenic approximation for complex atoms would satisfy the f-sum rule

but it would clearly be inaccurate. As demonstrated above, the CC-RM method is concerned primarily with the differential oscillator strength in the bf continuum that, in turn, depends on the delineation of autoionizing resonances.

Similarly, the RMO depends on the energy distribution monochromatic opacity via the Planck function at a given temperature. Fig. 3 (right) shows $\mathrm{d}B/\mathrm{d}T$ at the Z-pinch temperature of 2.11×10^6 K. Compared with the OP results, the distribution of the CC-RM Fe XVII monochromatic opacity is quite different and much more smoothed out, without the sharp variations that stem mainly from the treatment of resonances as bb lines (albeit inclusion of limited autoionization broadening perturbatively in the DW approximation). The flatter distribution is also observed experimentally in contrast to theoretical opacity models that exhibit "opacity windows" (see Fig. 3, left).

8. Plasma Broadening of Autoionizing Resonances

An unsolved atomic physics problem is the broadening of autoionizing resonances by plasma effects, in spite of line-broadening theory being well developed and extensively considered in existing opacity calculations. But since autoionizing resonance shapes are not considered, neither is their broadening as function of density and temperature. However, the distribution of differential oscillator strength and the structure of the bf opacity depends critically on how resonances broaden and dissolve into the continuum from the CC-RM calculations.

At high densities the dominant form of plasma broadening is due to electron impact. We have developed an algorithm implemented in the INTFACE code (see Fig. 2) prior to the opacity calculations (Pradhan et al. 2018). Fig. 4 shows the electron impact broadening of autoionizing resonances in a typical CC-RM photoionization cross section at two temperatures, 10^6 K and 10^7 K, and a range of densities: from $N_e = 10^{20}\,\mathrm{cm}^{-3}$, where the onset of broadening is discernible, to the high density $N_e = 10^{23}\,\mathrm{cm}^{-3}$ where the resonance structures are mostly dissolved into the continuum. The broadening profiles are normalized Lorentzian with no effect on the non-resonant continuum (viz. Fig. 3, right).

9. Equation of State

The MHD-EOS was formulated for the OP by Mihalas et al. (1988). The MHD "chemical picture" treats isolated atoms, for which the CC-RM data are computed, perturbed by the plasma environment via occupation probabilities w_i in the atomic internal partition function

$$U(i, j, k) = \sum_i w_i\, g_i\, \exp(-E_i/kT) \tag{6}$$

and the modified Boltzmann–Saha equation. E_i is the excitation energy of level i, g_i its statistical weight, and T the temperature. The w_i are determined upon the free-energy minimization of the plasma at a given temperature–density. An atomic level i is considered dissolved by the plasma microfield when its highest Stark sublevel overlaps with the lowest sublevel of the $i + 1$ level. The MHD-EOS originally stipulated a stringent validity criterion for mass densities $\rho \leq 0.01\ \mathrm{g\,cm}^{-3}$ valid for stellar envelopes (Seaton et al. 1994). But that is insufficient even to reach the solar BCZ depths with $\rho \geq 0.1\ \mathrm{g\,cm}^{-3}$. Nevertheless, a modified version named Q-MHD has been employed in

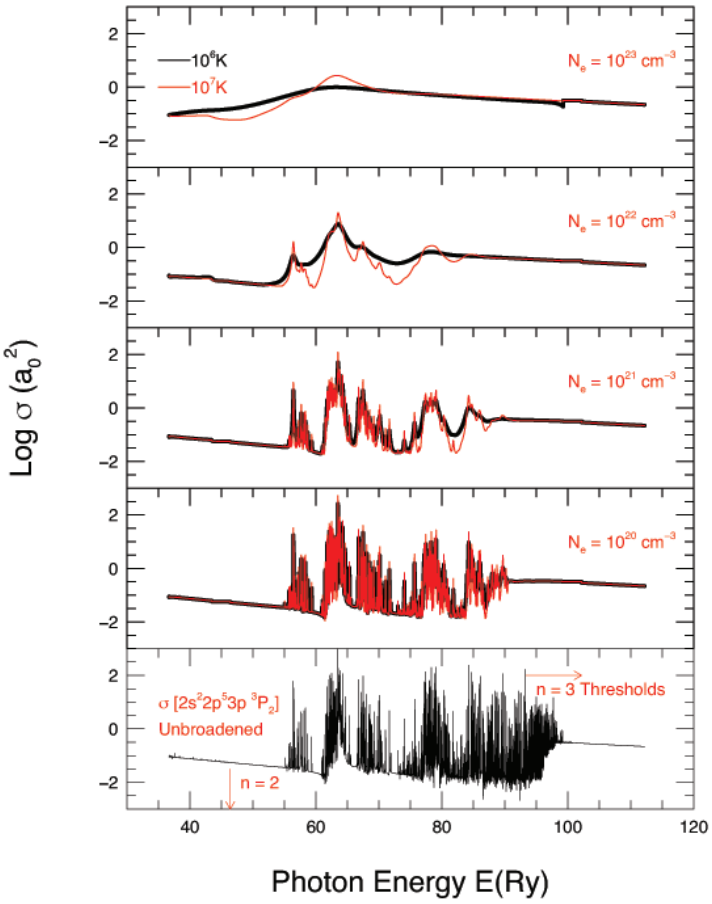

Figure 4. Plasma broadening of autoionizing resonances with temperature and densities. *Bottom panel*: unbroadened cross section. *Upper panels*: dissolution of resonance structures into the bf continuum with increasing density at $T = 10^6$ K (black) and 10^7 K (red).

the OP work with the W_i cutoffs at very high densities. An unresolved problem has also been that the chemical picture level populations are orders of magnitude lower (Badnell & Seaton 2003) than the physical picture EOS used in the OPAL opacity calculations (Rogers & Iglesias 1992). An improved treatment of these issues in the high-density regime has been developed by Trampedach et al. (2006), and will be incorporated in the new RM opacity calculations.

Another issue pertains to top-up levels referred to above. Including a large number of levels in the MHD-EOS drastically affects the overall population distribution since it is normalized via the internal partition function (Eq. 4). To wit: the ground state of Fe XVII ends up with no more than a few percent of the population at Z-pinch plasma and BCZ conditions. It is expected that the improved method by Trampedach et al. (2006) could also alleviate this problem.

10. Conclusion

The *R*-Matrix opacity calculations described in this review are difficult and time consuming but ensure high accuracy using state-of-the-art atomic physics, as originally envisioned in the OP. Furthermore, the CC-RM calculations are needed to verify existing opacity models that employ variants of the simpler DW method, but with large differences of ∼30% or more among them (viz. Table 1). Ongoing and planned laboratory experiments at the Sandia Z-pinch and the Livermore NIF (Perry et al., this volume) should also serve to validate theoretical models to resolve outstanding discrepancies and fundamental issues in atomic physics, astrophysics, and plasma physics.

Acknowledgments. We would like to thank Werner Eissner, Regner Trampedach, Lianshui Zhao, and Chris Orban for contributions. This work was partially supported by the US Department of Energy and the US National Science Foundation. The computational work was carried out primarily at the Ohio Supercomputer Center, Columbus.

References

Asplund, M., Grevesse, N., Sauval, A. J., & Scott, P. 2009, ARA&A, 47, 481
Badnell, N. R., & Seaton, M. J. 2003, J. Phys. B – At. Mol. Opt., 36, 4367
Bahcall, J. N., Basu, S., Pinsonneault, M. H., & Serenelli, A. M. 2005, ApJ, 618, 1049
Bailey, J. E., Nagayama, T., Loisel, G. P., et al. 2015, Nature, 517, 56
Basu, S., & Antia, H. N. 2008, Phys. Rep., 457, 217
Berrington, K. A., Burke, P. G., Seaton, M. J., et al. 1987, J. Phys. B – At. Mol. Opt., 20, 6379
Blancard, C., Colgan, J., Cosse, Ph. 2016, Phys. Rev. Lett., 117, 249501
Burke, P. G. 2011, *R*-Matrix Theory of Atomic Collisions: Application to Atomic, Molecular and Optical Processes (Berlin-Heidelberg, Germany: Springer-Verlag), vol. 61 of Springer Series on Atomic, Optical, and Plasma Physics
Christensen-Dalsgaard, J., Di Mauro, M. P., Houdek, G., & Pijpers, F. 2009, A&A, 494, 205
Delahaye, F., Zwölf, C. M., Zeippen, C. J., et al. 2016, J. Quant. Spectrosc. Ra., 171, 66
Eissner, W. 1991, in The Effects of Relativity in Atoms, Molecules, and the Solid State, edited by Wilson, S., Grant, I. P., & Gyorffy, B. L. (New York, NY: Plenum Press), 55
Eissner, W., Jones, M., & Nussbaumer, H. 1974, Comput. Phys. Commun., 8, 270
Hibbert, A. 1975, Comput. Phys. Commun., 9, 141
Iglesias, C. A., & Hansen, S. B. 2017, ApJ, 835, 284
Mendoza, C., Seaton, M. J., Buerger, P., et al. 2007, MNRAS, 378, 1031
Mihalas, D., Däppen, W., & Hummer, D. G. 1988, ApJ, 331, 815
Nahar, S. N., Pradhan, A. K., Eissner, W., & Chen, G. X. 2011, Phys. Rev. A, 83, 053417
Nahar, S. N., & Pradhan, A. K. 2016a, Phys. Rev. Lett., 116, 235003
— 2016b, Phys. Rev. Lett., 117, 249502
Pradhan, A. K., & Nahar, S. N. 2011, Atomic Astrophysics and Spectroscopy (Cambridge, UK: Cambridge University Press)
Pradhan, A. K., Nahar, S. N., Zhao, L., et al. 2018, in preparation
Rogers, F. J. & Iglesias, C. A. 1992, ApJS, 79, 507
Seaton, M. J. 1987, J. Phys. B – At. Mol. Opt., 20, 6431
Seaton, M. J., Yu, Y., Mihalas, D., & Pradhan, A. K. 1994, MNRAS, 266, 805
The Opacity Project Team, 1995, The Opacity Project (Bristol, UK: IOP Publishing), vol. 1
The Opacity Project Team, 1997, The Opacity Project (Bristol, UK: IOP Publishing), vol. 2
Trampedach, R., Däppen, W., & Baturin, V. A. 2006, ApJ, 646, 560
Turck-Chièze, S. 1998, Space Sci. Rev., 85, 125
Turck-Chièze, S., Couvidat, S., Piau, L., et al. 2004, Phys. Rev. Lett., 93, 211102
Yu, Y., & Seaton, M. J. 1987, J. Phys. B – At. Mol. Opt., 20, 6409
Zhao, L., Eissner, W., Nahar, S., & Pradhan, A. 2018, this volume